Available online at www.sciencedirect.com
SCIENCE DIRECT®
Journal of Petroleum Science and Engineering 41 (2004) 269–285
JOURNAL OF PETROLEUM SCIENCE & ENGINEERING
www.elsevier.com/locate/petrol

Numerical solution for natural gas production from methane hydrate dissociation

Goodarz Ahmadi[a,*], Chuang Ji[a], Duane H. Smith[b]

[a] *Department of Mechanical and Aeronautical Engineering, Clarkson University, Potsdam, NY 13699-5725, USA*
[b] *National Energy Technology Laboratory, Department of Energy, Morgantown, WV 26507-0880, USA*

Received 30 August 2002; accepted 8 September 2003

Abstract

This paper describes a one-dimensional model for natural gas production from the dissociation of methane hydrate in a confined reservoir by a depressurizing well. The approach accounts for the heat released by hydrate dissociation and convection–conduction heat transfer in the gas and hydrate zone. The system of governing equations is solved using a finite-difference scheme. For different well pressures and reservoir temperatures, the gas flow, the pressure and temperatures conditions in the reservoir are simulated. Distributions of temperature and pressure in the hydrate and gas regions and time evolutions of natural gas output also are evaluated. It is shown that the gas production rate is a sensitive function of well pressure. In addition, both heat conduction and convection in the hydrate zone is important. The simulation results are compared with the linearization approach and the shortcomings of the earlier approach are discussed.

Keywords: Hydrate; Natural gas production; Hydrate dissociation; Numerical model

1. Introduction

Hydrate is treated as a potential energy resource for the 21st century because a large amount of methane gas is trapped in hydrate reservoirs. In the past 30 years, considerable effort has been made for commercial production of natural gas from hydrate reservoirs (Englezos, 1993). Until now, all methods are still limited to experimental scale (Collett and Lee, 2000) except for one gas-hydrate field in Western Siberia, which was exploited successfully (Makogon, 1997).

To recover natural gas from hydrate dissociation, depressurization is an effective method which is based on breaking the temperature–pressure equilibrium conditions of hydrate. In the depressurization method, a well is drilled into the hydrate reservoir and the well pressure is kept sufficient low to lead to dissociation of hydrate and release of natural gas.

Extensive reviews of gas hydrate were reported by Englezos (1993), Makogon (1997) and Sloan (1998). Thermodynamic modeling of the hydrate dissociation process by depressurization has been studied by a number of authors. Makogon (1974, 1997) viewed hydrate dissociation as a moving boundary ablation process, and used the classical Stefan's equation to describe the process of hydrate dissociation. In this model, a dissociation front is assumed to exist to

* Corresponding author. Tel.: +1-315-268-2322; fax: +1-315-268-6438.
E-mail address: ahmadi@clarkson.edu (G. Ahmadi).

0920-4105/$ - see front matter © 2003 Elsevier B.V. All rights reserved.
doi:10.1016/j.profnurs.2003.09.004

separate the hydrate reservoir into a gas and a hydrate zone. Governing equations for the movement of natural gas in both zones are set up separately. A set of self-similar solutions for the pressure profiles was obtained after linearization of the governing equations. The water released during the hydrate dissociation was ignored in this model.

Verigin et al. (1980) developed Makogon's model by considering the gas and water mass balance at the dissociation front. The water released from the hydrate dissociation was assumed to be stationary and not to affect the flow of natural gas. In these earlier models, however, the process of hydrate dissociation was treated as an isothermal process.

Holder et al. (1982) simulated mass and heat transfer for the depressurization process in a hydrate reservoir overlaying a free natural gas zone. In this model, hydrate dissociation was assumed to occur only at the interface between hydrate "cap" and free natural gas layer. An energy equation involving only heat conduction was used to describe the temperature distribution in the natural gas layer. The continuity equation was used to describe the natural gas flow, in which the pressure gradient and the gas flow velocity were connected by Darcy's law. A heat balance at the interface of the hydrate "cap" and free natural gas layer was set up, from which the rate of hydrate dissociation was determined.

Water flow during the hydrate dissociation was considered by Burshears et al. (1986). They extended the model of Holder et al. (1982) by adding a mass balance of water at the dissociation front; however, the convective heat transfer in the area where gas and water coexist was not considered. Selim and Sloan (1989) studied a thermal stimulation method for hydrate dissociation. In their one-dimensional model, convective–conductive heat transfer was considered under the assumption that the water in the reservoir remained stationary and the well temperature was kept constant. An analytical expression for the temperature distribution in the reservoir was obtained.

Yousif et al. (1991) used a Kim–Bishnoi model (Kim et al., 1987) to describe a dissociation process of methane hydrate in Berea sandstone by depressurization. In a one-dimensional model, the hydrate dissociation process was assumed to be isothermal. Gas and water flow were all considered in separated continuity equations, pressure of gas and water was connected by capillary pressure. Variations of gas phase permeability and porosity during the hydrate dissociation also were considered. The results showed distributions of pressure and hydrate saturation and the movement of the hydrate dissociation interface. The experimental data of gas and water production matched the mathematical model quite well.

Kamath (1983) used thermal stimulation for hydrate dissociation and studied the enthalpy of dissociation for hydrates of different gases. Hydrates with different natural gas compositions dissociated with injection of hot water and the results showed that the rate of heat transfer and the rate of hydrate dissociation were power law functions of the temperature difference. A modified Clausius–Clapeyron equation was obtained to calculate hydrate dissociation enthalpy. This research also revealed additional details about the process of heat transfer at the hydrate dissociation interface.

Bondarev and Cherskiy (Makogon, 1997) further developed the model of Makogon (1974) by including the heat transfer process in the porous medium. The conductive–convective energy equations in the gas and hydrate zones were used and the effects of the throttling process were included. Makogon (1997) reported analytical expressions for the one-dimensional temperature and pressure profiles that were obtained after linearization of the governing equations. The model, however, neglected the heat balance at the dissociation front.

Tsypkin (2000) also assumed the presence of a dissociation front and separated the hydrate reservoir into hydrate and gas zones during hydrate dissociation by depressurization. In his multiphase one-dimensional model, movement of water and gas in the reservoir was described and heat and mass balance at the dissociation front were included. He obtained similarity solutions for temperature and pressure distributions by a perturbation method. Masuda et al. (1999) treated the process of hydrate dissociation as a Kim et al. (1987) kinetic process. In this model the driving force for hydrate dissociation is the difference between the equilibrium pressure and gas pressure. Their numerical results were in agreement with their experimental data. Moridis et al. (1998) added a module for hydrate dissociation into the TOUGH2 general-purpose reservoir simulator. The

flow of gas and water were considered and the conductive–convective heat transfer equation was used.

Durgut and Parlaktuna (1996) described a thermal stimulation method for natural gas production in a hydrate reservoir. Their two-dimensional model included heat conduction and convection, and both water and gas flows. More recently, Swinkels and Drenth (1999) studied the behavior of a hydrate-capped gas reservoir using a 3-D thermal reservoir simulator. They concluded that the simulation could provide insight into the natural gas production process and for economical evaluation of different production scenarios. They also noted that the gas production from the hydrate cap might become thermally limited.

Ahmadi et al. (2000) and Ji et al. (2001) used the combined models of Verigin et al. (1980) and Bondarev and Cherskiy as reported by Makogon (1997). In this model, a set of self-similar solutions for temperature and pressure was obtained after linearization of the governing equations. The results led to a system of coupled algebraic equations for the location of the dissociation front, and the temperature and pressure at the front. This system was solved by an iterative scheme. Numerical results for time evolutions of pressure and temperature profiles in the hydrate reservoir, as well as the location of the front and the natural gas production were obtained.

In this paper, the problem of natural gas production from a depressurizing well in hydrate reservoirs is studied. The case that the well pressure is fixed, reservoir is partially saturated with hydrate, and the reservoir contains pressurized natural gas is analyzed. The energy equation including both heat conduction and convection was used in the analysis. The mass balance and heat balance at the dissociation front are included in the analysis. Governing equations are solved using a finite-difference numerical scheme. For several well pressures and reservoir temperatures, numerical results for time evolutions of pressure and temperature profiles in the hydrate reservoir, as well the location of the front and the natural gas production rate are obtained. The results are compared with those obtained by the linearization method suggested by Makogon (Ji et al., 2001), and the shortcoming of the linearization method is discussed.

2. Hydrate dissociation model

Assume that there is a methane hydrate reservoir with pressure P_e and temperature T_e containing stable solid hydrate and free methane gas. When a well is drilled into the reservoir, the pressure in the drilled area drops to the well pressure P_G. For sufficiently low pressure P_G below the pressure–temperature equilibrium condition, the hydrate in the neighborhood of the well dissociates. The process of hydrate dissociation is assumed to be analogous to ice melting, which occurs at a front instead of the entire volume. The so-called dissociation front separates the reservoir into two zones. The gas zone forms near the well, where only natural gas and water exist. The hydrate zone is further away from the well, where the solid hydrate and natural gas exist. Natural gas can then be recovered from the well, while the dissociation front moves outward into the reservoir with time.

In the present study, it is assumed that the pressure and temperature at the dissociation front are respectively the equilibrium pressure, P_D, and temperature, T_D, which vary slowly with time. Water flow in the reservoir and the Joule–Thomson cooling effect are, however, neglected.

3. Mathematical model

Fig. 1 shows the one-dimensional model used in the computation. In this figure, the location of well is at $x=0$, where the well pressure is fixed at P_G. A length of $L=100$ m of the hydrate reservoir is modeled in the present analysis. At $x=L$, it is assumed that the reservoir pressure and temperature are, respectively, fixed at P_e and T_e. In this figure, the dissociation front, which is located at $X(t)$, separates the reservoir into two zones. The region $0<x<X(t)$ is referred to as the gas zone, and the area $X(t)<x<L$ is the hydrate zone. The dissociation front $X(t)$ moves outward as the gas production from the well continues.

In the subsequent analysis, subscript n identifies the region, with $n=1$ or 2 corresponding to the gas zone or the hydrate zone, respectively. Pressure distribution in the reservoir is governed by

$$\frac{\partial P_n}{\partial t} = a_n \frac{\partial^2 P_n^2}{\partial x^2} \tag{1}$$

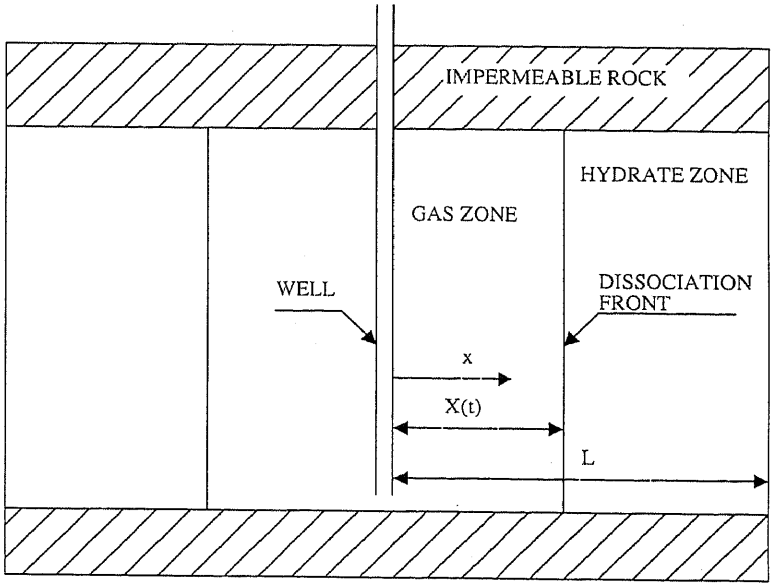

Fig. 1. Schematic of the hydrate reservoir for the one-dimensional model.

where

$$a_n = \frac{k_n}{\Phi_n \mu} \tag{2}$$

and

$$\Phi_1 = (1-\alpha)\Phi \tag{3}$$

$$\Phi_2 = (1-\beta)\Phi \tag{4}$$

Here P_n and k_n are the pressure and the gas permeability, respectively, μ is the gas viscosity, α is the water saturation, β is the hydrate saturation, Φ is the porosity, Φ_1 is the content of free gas in the gas zone, and Φ_2 is the content of free gas in the hydrate zone.

The velocity of natural gas v_n in the gas and the hydrate zones is given by Darcy's law, i.e.,

$$v_n = -\frac{k_n}{\mu}\frac{\partial P_n}{\partial x} \tag{5}$$

Assuming that the time variation of gas density is small, the heat transfer equation in the gas and hydrate zone is given as

$$\frac{\partial T_n}{\partial t} + v_n \frac{\partial T_n}{\partial x} = \alpha_n \frac{\partial^2 T_n}{\partial x^2} \tag{6}$$

where T_n is the temperature, and α_n is the heat diffusivity in the gas and hydrate zone.

In general, the equilibrium temperature and pressure at the dissociation front are functions of time. The phase equilibrium relation between temperature T_D and pressure P_D at the dissociation front is given as (Makogon, 1997)

$$\log_{10} P_D = a(T_D - T_0) + b(T_D - T_0)^2 + c \tag{7}$$

where T_0 is 273.15 K and a, b, c are empirical constants that depend on the hydrate composition. Values of a, b, and c are obtained from the equilibrium pressure–temperature data of methane hydrate. Using a least square fit, it follows that (Ji et al., 2001) $a=0.0342\ \mathrm{K}^{-1}$, $b=0.0005\ \mathrm{K}^{-2}$, $c=6.4804$ where in Eq. (7), P_D is in Pa.

The process of hydrate dissociation at the dissociation front is an endothermic phase-change process. The dissociation heat for per kilogram of hydrate in J/kg is given as (Kamath, 1983)

$$\Delta H = AT_D + B \tag{8}$$

where T_D is the dissociation temperature, and A, B are constants given by

$$A = -1050\ \mathrm{J/kg},\quad B = 3{,}527{,}000\ \mathrm{J/(kg\ K)}$$

The initial and boundary conditions are given as

$$P_1(0,t) = P_G \tag{9}$$

$$P_1(X(t),t) = P_2(X(t),t) = P_D(t) \tag{10}$$

$$T_1(X(t),t) = T_2(X(t),t) = T_D(t) \tag{11}$$

$$P_2(L,t) = P_2(x,0) = P_e \tag{12}$$

$$T_2(L,t) = T_2(x,0) = T_e \tag{13}$$

Energy balance at the dissociation front is given by

$$v_1(X,t)\rho_1(X,t)C_P T_1(X,t) - v_2(X,t)\rho_2(X,t) \times C_P T_2(X,t) - K_1 \frac{\partial T_1}{\partial x}|_{x=X} + K_2 \frac{\partial T_2}{\partial x}|_{x=X} = \Delta H \dot{m}_h \tag{14}$$

where K_n is the heat conductivity in the gas and hydrate zone, ρ_n is the density of natural gas in zone 1 or 2, $\dot{m}_h$ is the hydrate dissociation rate per unit area, and C_P is the heat capacity of natural gas. In Eq. (14), the first term on the left hand side is the convective heat flux out of the dissociation front into the gas zone; the second term is the convective heat flux from the hydrate zone into the dissociation front. The third term is conductive heat flux from the dissociation front to gas zone. The fourth term is the conductive heat flux from hydrate zone into the dissociation front. The term on the right hand side is the rate of heat supplied for hydrate dissociation per unit time per unit area.

The densities of the natural gas in the gas and hydrate zone at the dissociation front are the same and are given as

$$\rho_1(X,t) = \rho_2(X,t) = \rho_0 \frac{P_D T_0}{z P_0 T_D} \tag{15}$$

where z is the gas compressibility, and ρ_0 is the gas density at atmospheric pressure P_0 and temperature T_0.

The mass rate of hydrate dissociation is given by

$$\dot{m}_h = \rho_3 \Phi \beta \frac{dX}{dt} \tag{16}$$

where ρ_3 is hydrate density, (dX/dt) is the speed of the dissociation front movement, and, as noted before β is hydrate saturation.

Substituting Eqs. (15) and (16) into Eq. (14), it follows that

$$v_1(X,t) - v_2(X,t) - \frac{zP_0K_1}{C_P\rho_0P_DT_0}\frac{\partial T_1}{\partial x}|_{x=X} + \frac{zP_0K_2}{C_P\rho_0P_DT_0}\frac{\partial T_2}{\partial x}|_{x=X} = \Delta H \frac{z\rho_3 P_0 \Phi\beta}{C_P\rho_0P_DT_0}\frac{dX}{dt} \tag{17}$$

The mass balance at the dissociation front is given as

$$\rho_1 v_1(X,t) - \rho_2 v_2(X,t) = -[\beta\varepsilon\rho_3 - (1-\alpha)\rho_1]\Phi\frac{dX}{dt} \tag{18}$$

where ε is the mass fraction of gas in methane hydrate.

Using Eq. (15), Eq. 18 may be restated as

$$v_1(X,t) - v_2(X,t) = -[\varepsilon\beta\frac{\rho_3 P_0 T_D}{\rho_0 P_D T_0} z - (1-\alpha)]\Phi\frac{dX}{dt} \tag{19}$$

Eqs. (7), (8), (17) and (19) describe the mass and energy balance at the dissociation front.

4. Numerical method of solution

In the numerical simulation, initially the length of reservoir is 100 m, which is divided into 500 grids. That is, a grid spacing of 0.2 m is used. To start the computation, it is assumed that the dissociation front is formed with a 1-m-long gas zone. The temperature and pressure profiles in the gas zone at the initial time are assumed to be linear.

Eqs. (1) and (6) are four coupled equations governing the temperature and pressure variations in the reservoir. These equations are non-dimension-sized and solved with a finite-difference method as described in Appendix A. An explicit central difference method is used to solve the pressure Eq. (1) and an upwind explicit method is used to solve heat transfer Eq. (6) in the gas zone. To solve the conduction–convection heat transfer Eq. (6) in the hydrate zone, an implicit method is used. Details of the finite-

difference forms of the governing equations are given in Appendix A.

The dissociation front $X(t)$ is a moving boundary at the interface between the hydrate and the gas zones. At the initial time, T_D and P_D are unknown. The correct values of T_D and P_D must satisfy the balance of energy and mass given by Eqs. (17) and (19). A bisection method is used to obtain the correct P_D and T_D at the dissociation front. At the start, the values of P_D and T_D, are assumed; Eqs. (1) and (6) are then solved iteratively for 20 h, which is the estimated time for forming a 1-m-long gas zone. The velocity of dissociation front motion, (dX/dt), is then evaluated from both Eqs. (17) and (19). The initially assumed values for P_D, T_D are adjusted until the values of (dX/dt) obtained from Eqs. (17) and (19) are the same within a specified tolerance.

In the computation, values of (dX/dt) are evaluated from Eqs. (17) and (19) at every time step and are compared. The bisection method is then used to adjust $T_{D(t)}$ and $P_{D(t)}$ until the values of (dX/dt) become the same (with the specified tolerance). Since the dissociation temperature T_D and pressure P_D are slowly varying functions of time, only a few iterations are needed to find a converge solution for the velocity of dissociation front.

At each time step, the dissociation front moves outward a small step $\Delta X(t)$. In the computation, the front is kept at the same grid until the accumulated motion of the front reaches one-grid length (0.2 m). Then the front is moved by one grid in the computational domain. To simulate an unbound reservoir, the length of the computational domain of the hydrate zone is kept fixed. As the dissociation front moves outward, the outer boundary of the hydrate reservoir also is moved by the same distance. That is, at the step that the dissociation front moves one grid, the gas zone becomes one grid longer and hydrate zone has the same length. The new dissociation temperature and pressure are then obtained by the bisection method, and the computation scheme continues.

5. Results

This section presents the numerical solution results for time evolutions of pressure and temperature profiles in the hydrate reservoir under various conditions. In addition, time variations of methane gas production, and location of the dissociation front also are evaluated. The values of the parameter used in the numerical simulation are listed in Appendix B.

For a reservoir temperature of 287 K, and a reservoir pressure of 15 MPa, Fig. 2 shows variations of pressure and temperature profiles at different times. Here the permeability in hydrate and gas zones are, respectively, 0.6 and 2.4 md. As noted before, the hydrate reservoir is divided into two zones by the dissociation front, and the temperature variations in the two zones are quite different. Fig. 2a shows that in hydrate zone, the temperature decreases gradually from the reservoir temperature far from the front to the dissociation temperature at the front. In the region near the dissociation front, the gradient of temperature variation becomes sharp, indicating a sharp increase in the heat conduction to the front. In the gas zone, temperature decreases gradually from the dissociation temperature at the dissociation front to its minimum value at the well. For different times, the temperature profiles in the gas region from well to the dissociation front remains roughly the same. Fig. 2a also shows that as the dissociation front moves outward, the temperature at the dissociation front, T_D, increases slightly with time. The time dependence of dissociation temperature observed here is in contrast to the result obtained from the linearization method suggested by Makogon (Ji et al., 2001), which leads to constant T_D.

The corresponding pressure profiles for different times under the same conditions for the far field and the near field are presented in Fig. 2b. The pressure decreases gradually from the reservoir pressure to the dissociation pressure at the dissociation front, and then decreases to its minimum value at the well. For the present case where the permeability of the gas zone is four times that of the hydrate zone, there is a sharp change in the slope of the pressure profile at the dissociation front as can be seen in Fig. 2b. This figure shows that the pressure profile in the gas region from well to the dissociation front remains unchanged.

For a reservoir pressure of 15 MPa, time evolutions of the gas mass flux (kg/m^2 s) across the reservoir are displayed in Fig. 2c. In the gas zone, the gas mass flux is nearly fixed, while in the hydrate zone, the gas mass flux increases towards the dissociation front. Fig. 2c

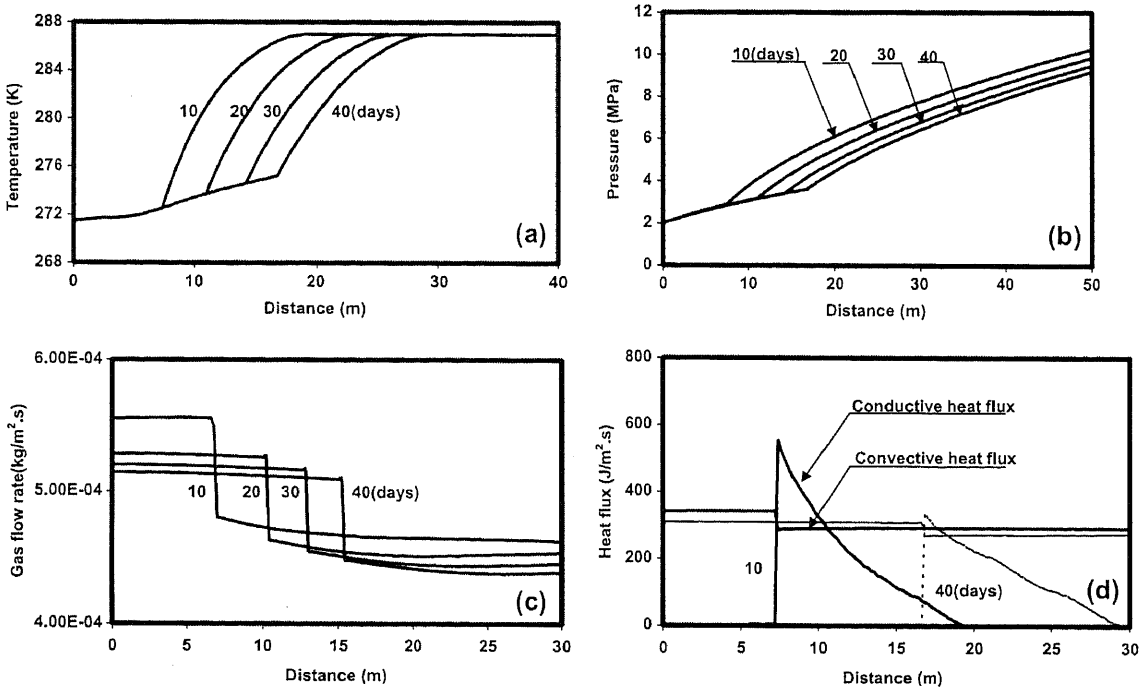

Fig. 2. Time variations of temperature, pressure, mass and heat flux profiles in a reservoir for a well pressure of 2 MPa and a reservoir temperature of 287 K.

shows that there is a jump in the mass flux due to the hydrate dissociation, which moves outward with time as the dissociation front penetrates deeper into the hydrate reservoir. The gas mass flux in the reservoir and the amount of natural gas generated due to hydrate dissociation decrease with time.

To provide an understanding of the nature of the hear transfer during hydrate dissociation, the heat flux profiles throughout the reservoir are shown in Fig. 2d. In this figure, the conductive and the convective heat fluxes are displayed separately at different times. Here solid lines show the profiles at 10 days, while the 40-day profiles are shown by dashed lines. In the hydrate zone, the conductive heat flux is very small in the region far away from the dissociation front, but increases sharply in the region near the dissociation front due to the large temperature gradient. In the gas zone, the conductive heat is negligibly small. The convective heat flux in both hydrate and gas zones are roughly constant. There is a jump of convective heat flux at the dissociation front, which indicates that the convective heat flow out of the dissociation front is always larger than the convective heat flow into the dissociation front. This is due to the added mass of gas that is generated at the dissociation front. Fig. 2d also shows that both convective heat flux and conductive heat flux decrease with time.

Comparisons of temperature, pressure and gas flow profiles as predicted by the present numerical method with the linearization method suggested by Makogon (Ji et al., 2001) are presented in Fig. 3. Here a reservoir temperature of 287 K, a reservoir pressure of 15 MPa and a well pressure of 2 MPa are used and all other parameters are kept identical. In these figures, the solid lines show the numerical simulation results, while the dashed lines show those of the linearized method. From Fig. 3a, it is seen that both temperature profiles reach the same boundary conditions far from the front, however, near the dissociation front, the temperature profiles of the numerical method have much sharper gradient when compared with that of the linearization method. The reason is that in linearization method suggested by Makogon, the heat conduction was ignored.

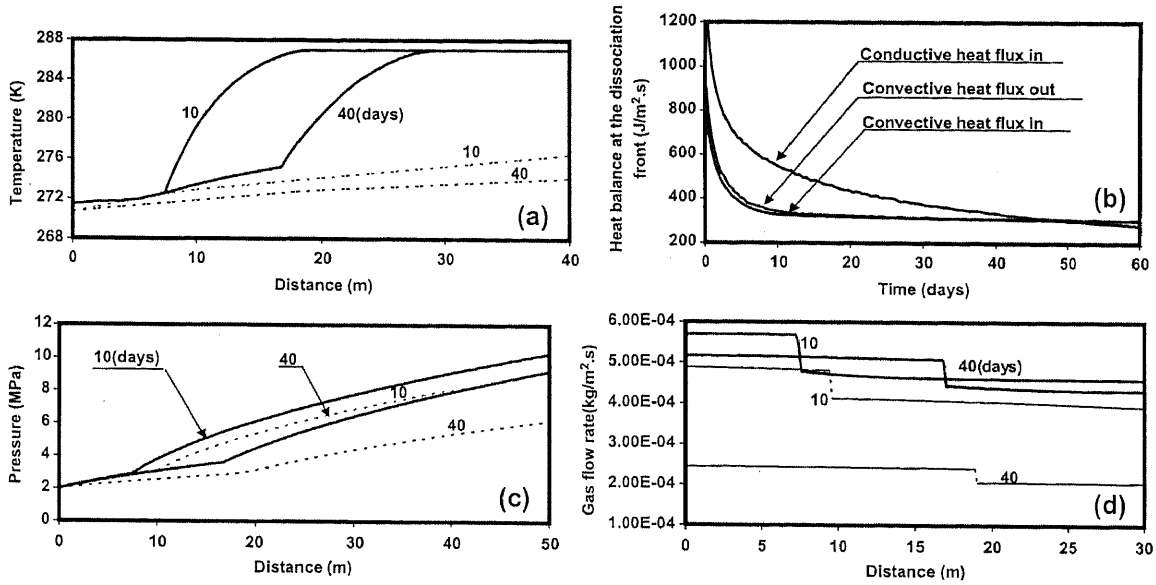

Fig. 3. Comparison of temperature and pressure profiles and mass flow rate with linearized solutions for a reservoir temperature of 287 K and a well pressure of 2 MPa. Solid lines: numerical solutions; dashed lines: linearized solutions suggested by Makogon (Ji et al., 2001).

To solve a conductive–convective heat transfer equation, two boundary conditions are needed. For solving Eq. (6), one boundary condition is given by Eq. (13), and the other is given by Eq. (11). The unknown dissociation temperature T_D, is obtained from the energy balance at the dissociation front given by Eq. (17). The linearization model suggested by Makogon (Ji et al., 2001), which neglects the heat conduction effects, requires only one boundary condition, which is given by Eq. (13). Thus, the energy balance at the dissociation front could not be included in the linearization model, which is a severe limitation of the linearization approach. In the absence of heat conduction, the temperature gradient in hydrate zone near the dissociation front becomes small.

To show the role of various heat fluxes at the dissociation front, time variations of conductive heat flux into the dissociation front, convective heat fluxes in and out of dissociation front are shown in Fig. 3b. It is clear that the convective heat flux into the dissociation front is roughly equal to the convective heat flux out of the front. This means that the conductive heat flux plays the dominant role in supplying the heat for hydrate dissociation. Fig. 3b implies that without the heat conduction, the energy balance at the dissociation front cannot be satisfied.

Fig. 3c compares the numerically predicted pressure profiles with those obtained by the linearization method. While the trends of the pressure profiles are comparable, there are quantitative differences. In the hydrate zone, the pressure as predicted by the linearization method is somewhat lower than that of the numerical method. In the linearization method, Eq. (1) is linearized with reservoir pressure P_e in the hydrate zone or well pressure P_G in the gas zone. Because the dissociation pressure P_D is close to P_G, the linearization does not alter the pressure profiles in the gas zone. While in the hydrate zone, the large difference between P_D and P_e leads to noticeable differences in the computed pressures by the two methods. Fig. 3c implies that the linearization method leads to pressure profiles that are qualitatively comparable to those obtained by the numerical method, with amount of error being larger in the hydrate zone.

Comparison of the mass flux (ρv) profiles of the numerical and the linearization methods is shown in Fig. 3d. For both methods, the predicted trends of mass flux profiles throughout the reservoir are similar; however, mass flux of the linearization method is lower than that of the numerical method. The reason is that the velocity, as given by Darcy's law, is proportional to the pressure gradient, and density is

proportional to the ratio of pressure over temperature. At a fixed time, Fig. 3 shows that the temperature and pressure of the numerical method are higher than that of the linearization method. Furthermore, pressure gradient in the hydrate zone is much larger than that of linearization method. The combined effects of a larger pressure gradient and a higher temperature and pressure of the numerical method lead to a higher mass flux throughout the reservoir.

For a well pressure of 1 MPa and reservoir temperature of 287 K, Fig. 4a presents temperature profiles at different times. Similar to Fig. 2a, the dissociation front divides the reservoir into the gas and the hydrate zones. The gradients of temperature in two zones are different. In the gas zone, the temperature decreases gradually from the dissociation temperature at the front to the temperature at the well. In the hydrate zone, the temperature decreases gradually from the reservoir temperature far from the dissociation front and sharply decreases to dissociation temperature in the region near the dissociation front. Fig. 4a also shows that the temperature in the gas zone varies slightly with time. Compared with Fig. 2a, the dissociation temperature at the dissociation front is lower and the dissociation front moves faster due to a lower well pressure. The corresponding pressure profiles are shown in Fig. 4b. Except for the lower dissociation pressures and the faster movement of the dissociation front, these profiles are quite similar to those shown in Fig. 2b.

Fig. 4c shows the time evolutions of the gas mass flux (kg/m^2 s) across the reservoir. In the gas zone, mass flux is roughly fixed, while in the hydrate zone, it increases towards the dissociation front. There is a jump in the mass flux at the dissociation front due to the hydrate dissociation. Comparing Figs. 4 and 2 shows that in the gas zone, the mass flux at lower well pressure is higher. In the hydrate zone, however, the mass fluxes in both figures are nearly the same. The jump of mass flux in Fig. 4c is larger than that in Fig. 2c, which indicates that under the same conditions, a lower well pressure leads to a higher rate of hydrate dissociation.

Fig. 4d presents the heat flux profiles throughout the reservoir. Here the conductive heat flux and convective heat flux are also shown separately at different times. The trends of heat flux profiles in

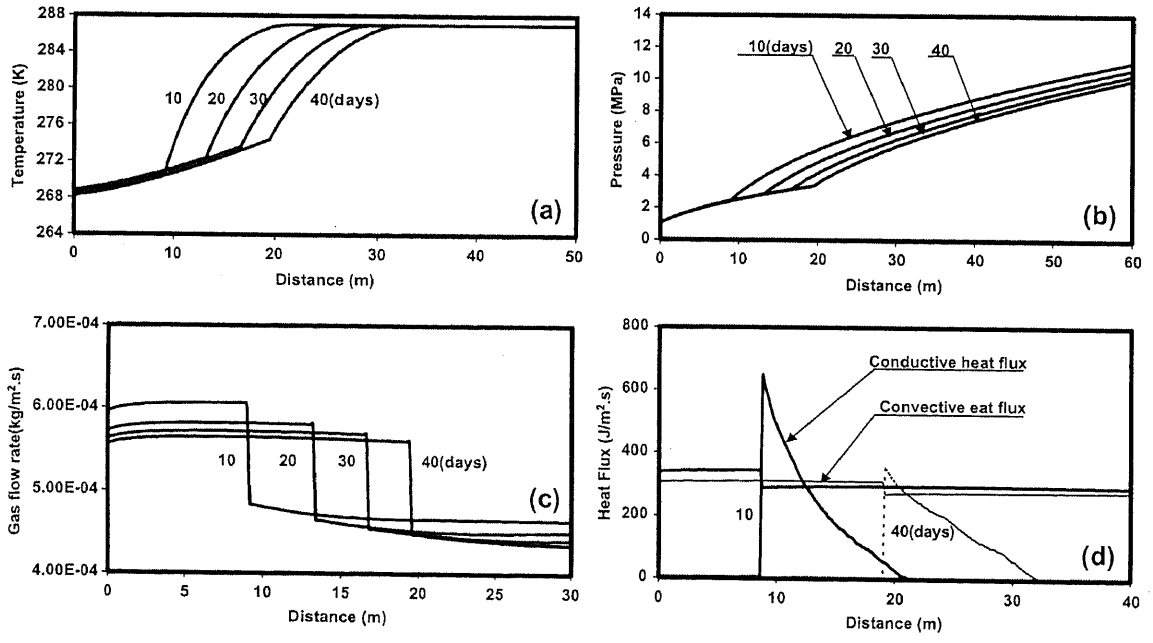

Fig. 4. Time variations of temperature, pressure, mass and heat flux profiles in a reservoir for a well pressure of 1 MPa and a reservoir temperature of 287 K.

Fig. 4d are similar to those shown in Fig. 2d. The conductive heat flux varies sharply in the region near the dissociation front and is higher than that shown in Fig. 2d. Fig. 4d shows that the convective heat flux, in the gas zone, is slightly higher than that of Fig. 2d, while in the hydrate zone, they are nearly identical.

For a reservoir with a temperature of 285 K and a well pressure of 2 MPa, the temperature, pressure, mass and heat flux profiles are shown in Fig. 5. The gas permeabilities in the gas zone and the hydrate zone are kept fixed at 2.4 and 0.6 md. Fig. 5a shows that the temperature profiles have trends similar to those shown in Fig. 2a. The only difference is that temperature in the gas zone noticeably decreases with time. Similarly, the pressure profiles shown in Fig. 5b are nearly the same as those shown in Fig. 2b. The dissociation front, however, moves slower in Fig. 5. Fig. 5c displays the mass flux profiles for the lower reservoir temperature. Comparing Figs. 5c and 2c shows that the difference of mass flux profiles in two figures are very small. This indicates that the effect of small variation of reservoir temperature on the gas flux is rather small.

Fig. 5d shows the time variation of total heat flux (sum of the conductive and convective heat fluxes). In the gas zone, the heat flux is nearly the same. In the hydrate zone far from the dissociation front, the heat flux, which is primarily convective heat flux, is roughly constant or increases slightly toward the dissociation front. In the region near-front, as the temperature decreases sharply to the dissociation temperature at the front, the conductive heat flux becomes quite large and the total heat flux increases sharply to the maximum value at the dissociation front. There is a jump of heat flux at dissociation front, which supplies the heat needed for hydrate dissociation. Fig. 5d also shows that the total heat flux decreases with time.

When the reservoir temperature is 283 K and all other conditions are identical, the temperature, pressure, mass and heat flux profiles are presented in Fig. 6. Fig. 6a and b shows that the temperature and pressure profiles are similar to those shown in Fig. 5a and b; except that the dissociation front moves slightly slower and the dissociation temperature and pressure are lower. The mass flux profiles shown in Fig. 6c are nearly the same as those shown in Fig.

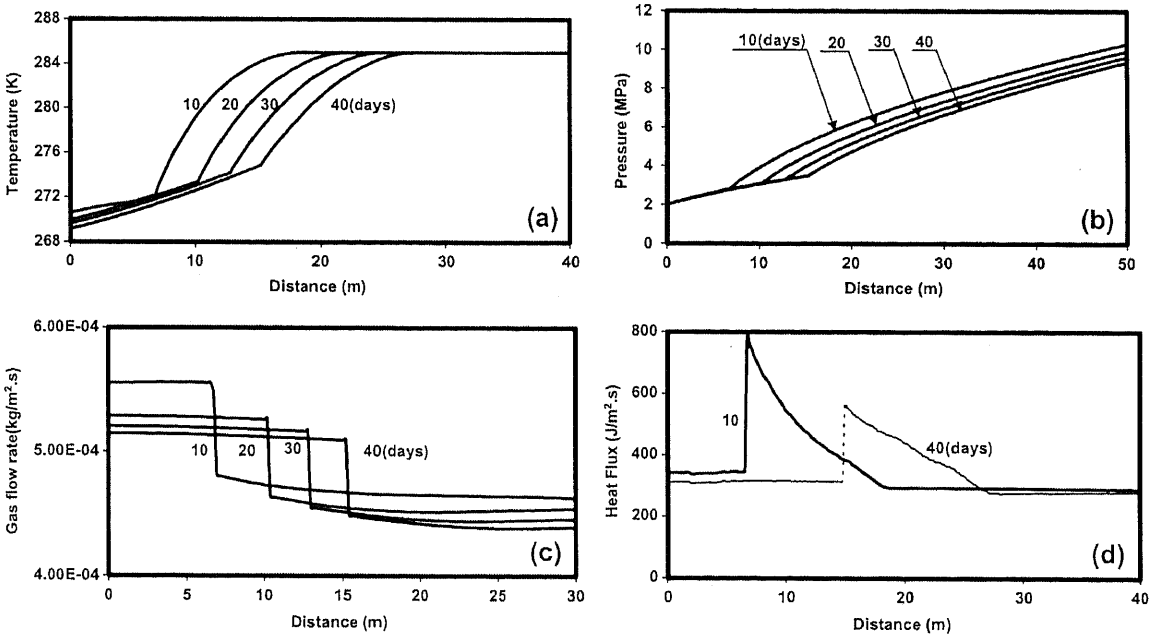

Fig. 5. Time variations of temperature, pressure, mass and heat flux profiles in a reservoir for a well pressure of 2 MPa and a reservoir temperature of 285 K.

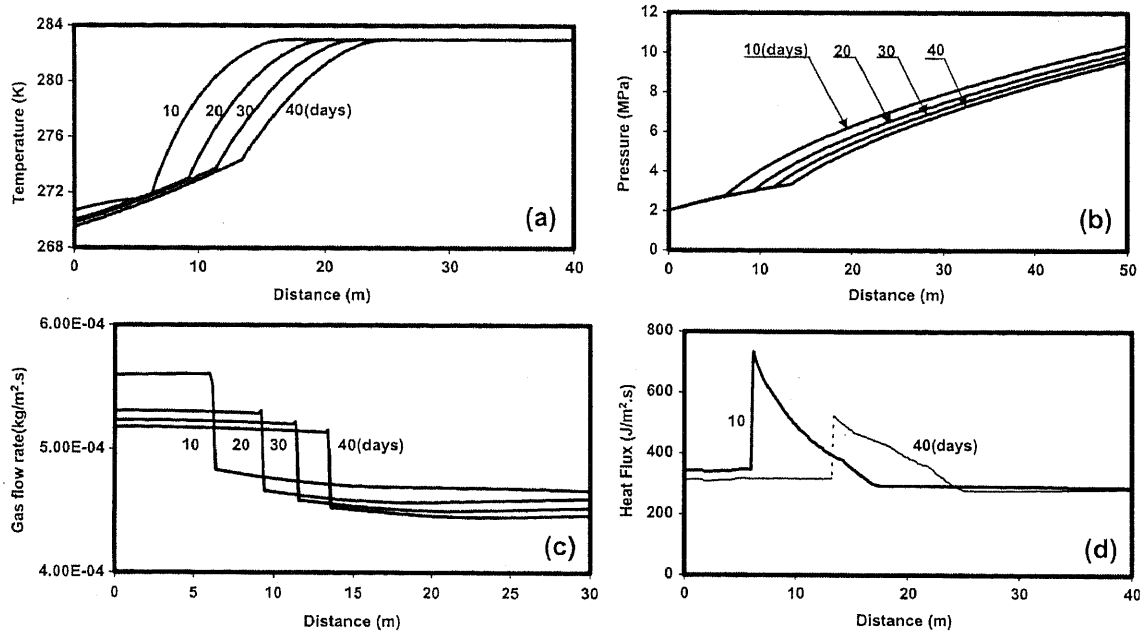

Fig. 6. Time variations of temperature, pressure, mass and heat flux profiles in a reservoir for a well pressure of 2 MPa and a reservoir temperature of 283 K.

5c, which again indicates that mass flux profile is not sensitive to small variation in the reservoir temperature. Fig. 6d shows the total heat flux at different times. Comparing Figs. 6d and 5d shows that for a lower reservoir temperature, heat flux in the region near dissociation front in the hydrate zone is smaller. This implies that reservoir temperature affects the temperature gradient in the region near the front.

For numerical and linearization methods, time variations of movement of dissociation front, natural gas output and dissociation temperature for different well pressures are compared in Fig. 7. The reservoir conditions are assumed to be fixed at 15 MPa and 287 K. The gas permeabilities in the gas and the hydrate zones are, respectively, 2.4 and 0.6 md. Numerical solutions are shown by solid lines, while the linearized solutions are shown by dashed lines. Fig. 7a shows the outward movement of the dissociation front with time. This figure indicates that as the well pressure decreases, the motion of the front speeds up. For a well pressure of 3 MPa, the movement of the dissociation front as predicted by the linearization method is comparable to that of the numerical method. For the linearization method, however, the motion of the dissociation front is more sensitive to well pressure when compared with that of the numerical method. When the well pressure decreases to 1 MPa, the lineaerization method predicts that the dissociation front moves twice as fast, while the numerical method predicts only a 30% increase.

Time evolutions of the natural gas output are plotted in Fig. 7b. The natural gas output decreases with time, and also decreases as the well pressure increases. The natural gas output as predicted by the numerical method appears to level-off or decreases very slightly after the initial transient. For a fixed well pressure, the gas output as evaluated by the linearization method is lower than that of the numerical method and continues to decrease with time.

Fig. 7c shows time variations of the dissociation temperature for different well pressures. For a fixed well pressure, the dissociation temperature as predicted by the numerical method increases with

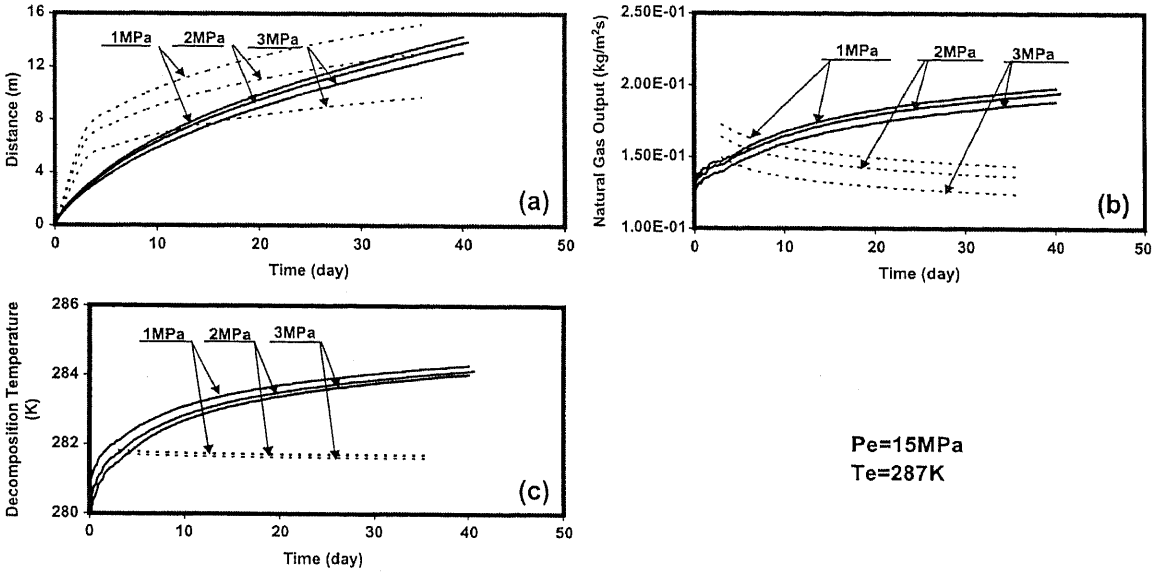

Fig. 7. Comparison of variations of the position of dissociation front, natural gas output and dissociation temperature with linearized solutions for different well pressures. Solid lines: numerical solutions; dashed lines: linearized solutions suggested by Makogon (Ji et al., 2001).

time. The slight fluctuation of the dissociation temperature at the beginning is related to the assumed initial start up conditions in the reservoir. The dissociation temperature of the numerical method also varies with the well pressure, and increases as the well pressure increases. The linearization method, however, leads to the dissociation temperature that is independent of time (Makogon,

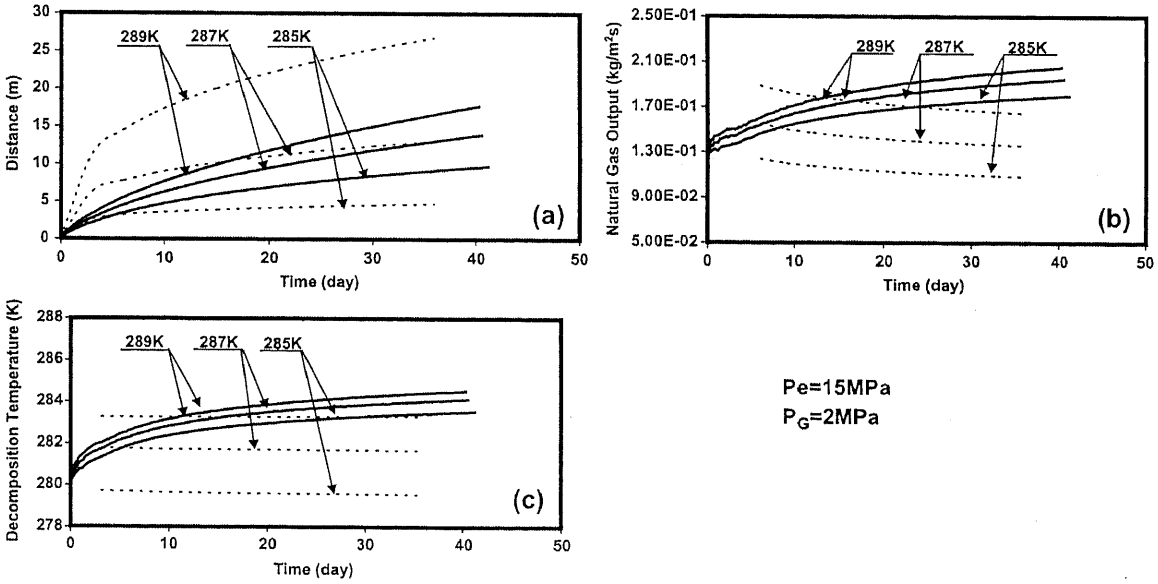

Fig. 8. Comparison of the variations of the position of dissociation front, natural gas output and dissociation temperature with linearized solutions for different reservoir temperatures. Solid lines: numerical solutions; dashed lines: linearized solutions suggested by Makogon (Ji et al., 2001).

1997; Ji et al., 2001), and is not as sensitive to well pressure.

For different reservoir temperatures, Fig. 8 compares time variations of the movement of the dissociation front, natural gas output and the dissociation temperature as predicted by the numerical method with those of the linearization method. Here the reservoir and well pressures of 15 and 2 MPa are assumed and the values of all other parameters are kept the same as those used in Fig. 7. Fig. 8a shows the movement of the dissociation front. It is seen that the dissociation front moves faster when the reservoir temperature increases. The linearization method, however, predicts a sharp variation of the dissociation front motion when compared with the numerical method.

In Fig. 8b, time variations of the natural gas output for different reservoir temperatures are presented. The numerical method predicts that the natural gas output increases slightly with time and is not very sensitive to the reservoir temperature. The linearization solution, however, leads to a slightly decreasing trend. The reason is that the natural gas production depends on the pressure gradient near the well, which is not significantly affected by reservoir temperature. It also observed that the natural gas output predicted by the linearization method is smaller than that of the numerical method for a fixed reservoir temperature.

Fig. 8c shows time variations of the dissociation temperature with the reservoir temperature. The numerical method predicts that the dissociation temperature increases with time and the reservoir temperature. The linearization method, however, leads to a time-independent dissociation temperature that varies significantly with the reservoir temperature.

6. Summary

A one-dimensional model for natural gas production form hydrate dissociation by depressurization is presented. The equations governing the pressure and temperature fields in the reservoir, and balance of energy and mass flux at the dissociation front, are solved using a finite-difference method. Time evolutions of temperature, pressure, gas mass flow and heat flux profiles across the reservoir, as well the movements of dissociation front and the natural gas output are evaluated. The results are compared with those of the linearized solutions suggested by Makogon (1997) and Ji et al. (2001). On the basis of the presented results, the following conclusions may be drawn:

1. The presented one-dimension model suggests that, under favorable hydrate reservoir conditions, depressurization (by drilling well) is a viable method producing natural gas from hydrate reservoirs.
2. For a fixed reservoir condition, well pressure controls the rate of natural gas output and the motion of the dissociation front. A lower well pressure leads to a higher natural gas output rate and a faster movement of the dissociation front.
3. Reservoir temperature affects the motion of dissociation front; however, the natural gas output is not sensitive to small variation in the reservoir temperature.
4. The dissociation temperature and pressure are slowly varying functions of time.
5. The dissociation temperature and pressure increase with the well pressure and the reservoir temperature.
6. Compared to the linearization method used in Makogon's model, the numerical method introduced in this paper provides a more accurate description for the process of hydrate dissociation.
7. The linearization method neglects the balance of energy at the dissociation front, which is included the presented numerical model.
8. The finite-difference approach is advantageous in that it does not require linearization of the governing equations and also includes balance of energy at the dissociation front.

Due to the difficulty associated with the semi-analytical linearization model, its extension to multi-dimensions may not be meaningful, and should be critically evaluated.

Acknowledgements

The financial support of the National Energy Technology Laboratory, US Department of Energy is gratefully acknowledged.

Appendix A. Finite-difference forms of the governing equations

A.1. Nondimensional governing equations

For the sake of numerical simulation, it is advantageous to restate the governing equations (Eqs. (1), (6) and (7)) in non-dimensional form. Introducing non-dimensional variables

$$x^* = \frac{x}{L} \quad P_n^* = \frac{P_n}{P_e} \quad T_n^* = \frac{T_n}{T_e} \quad t^* = a_1 \frac{P_e t}{L^2} \tag{A1}$$

Here superscript * donates the dimensionless variables, x^* is the non-dimensional distance, P_n^* and T_n^* are the non-dimensional pressure and temperature in the gas and the hydrate zones, and t^* is the non-dimensional time.

Using Eq. (A1), Eq. (1) in non-dimensional form may be restated as

$$\frac{\partial P_1^*}{\partial t^*} = \frac{\partial^2 P_1^{*2}}{\partial x^{*2}} \tag{A2}$$

$$\frac{\partial P_2^*}{\partial t^*} = \frac{a_2}{a_1} \frac{\partial^2 P_1^{*2}}{\partial x^{*2}} \tag{A3}$$

Eqs. (A2) and (A3) govern the nondimensional pressure in the gas and the hydrate zones, respectively. Similarly, the non-dimensional form of Eq. (6) is given as

$$\frac{\partial T_1^*}{\partial t^*} - \frac{k_1}{\mu} \frac{\partial P_1^*}{\partial x^*} \frac{\partial T_1^*}{\partial x^*} = A_1 \frac{\partial^2 T_1^*}{\partial x^{*2}} \tag{A4}$$

The non-dimensional form of Eq. (7) is given as

$$\frac{\partial T_2^*}{\partial t^*} - \frac{k_2}{\mu} \frac{\partial P_2^*}{\partial x^*} \frac{\partial T_2^*}{\partial x^*} = A_2 \frac{\partial^2 T_2^*}{\partial x^{*2}} \tag{A5}$$

where

$$A_2 = \frac{\alpha_2}{P_e a_1} \tag{A6}$$

The boundary conditions given by Eqs. 10–14 may be restated as

$$P_1^*(0, t^*) = \frac{P_G}{P_e} \tag{A7}$$

$$P_1^*(X^*, t^*) = P_2^*(X^*, t^*) = \frac{P_{D(t^*)}}{P_e} \tag{A8}$$

$$T_1^*(X^*, t^*) = T_2^*(X^*, t^*) = \frac{T_{D(t^*)}}{P_e} \tag{A9}$$

$$P_2^*\left(1 + \frac{dX^*}{dt^*}, t^*\right) = 1 \tag{A10}$$

$$T_2^*\left(1 + \frac{dX^*}{dt^*}, t^*\right) = 1 \tag{A11}$$

where X^* is the non-dimensional location of the dissociation front, which is a function of time.

The assumed initial conditions are restated as

when $0 < x^* < X^*$,

$$T_1^*(x^*, 0) = \frac{T_{D(0)}}{T_e} + \frac{x^* - X^*}{X^*} \frac{T_{D(0)} - T_{G(0)}}{T_e} \tag{A12}$$

when $0 < x^* < X^*$,

$$P_1^*(x^*, 0) = \frac{P_{D(0)}}{P_e} + \frac{x^* - X^*}{X^*} \frac{P_{D(0)} - P_G}{P_e} \tag{A13}$$

when $X^* < x^* < 1$, $T_2^*(x^*, 0) = 1$ (A14)

when $X^* < x^* < 1$, $P_2^*(x^*, 0) = 1$ (A15)

where $T_{G(0)}$ is the well temperature assumed at the initial time. Simulation results were found to be insensitive to the assumed value of $T_{G(0)}$.

A.2. Finite-difference forms

The computation region is divided into 500 grids. The well is located at grid 1 and the outer boundary

is located at grid 501. The location of the dissociation front is at grid I_1, which varies with time. To solve Eq. (A2), a central finite-difference method is used. Accordingly,

$$P_{1i}^{*n+1} = \frac{\Delta t^*}{\Delta x^{*2}}\left(P_{1(i+1)}^{*2} + P_{1(i-1)}^{*2} - 2P_{1i}^{*2}\right) + P_{1i}^* \tag{A16}$$

where Δt^* is the non-dimensional time step and Δx^* is the non-dimensional step in space. In Eq. (A16), the first subscript "1" denotes the gas zone, the second subscript "i" corresponds to the computation grid i, which ranges from 2, to $I_1 - 1$ (the grid before the position of the dissociation front). The superscript $n+1$ refers to the value of pressure at the next time step $n+1$.

The central finite differencing form of (Eq. A3) is given as

$$P_{2i}^{*n+1} = \frac{a_2}{a_1}\frac{\Delta t^*}{\Delta x^{*2}}\left(P_{2(i+1)}^{*2} + P_{2(i-1)}^{*2} - 2P_{2i}^{*2}\right) + P_{2i}^* \tag{A17}$$

The definition of subscripts and superscripts are the same as in (Eq. A16). Except subscript "2" denotes the hydrate zone. The computation domain is from the grid $I_1 + 1$ to N.

Eq. (A4) is solved by an explicit upwind differencing method. That is

$$T_{1i}^{*n+1} = -\frac{k_1}{\mu}\frac{\Delta t^*}{\Delta t^{*2}}\left(P_{1(i+1)}^* - P_{1i}^*\right)\left(T_{1(i+1)}^* - T_{1i}^*\right) + \text{source}_i \tag{A18}$$

where

$$\text{source}_i = \frac{A_1\left(T_{i+1}^{*n} + T_{i+1}^{*n} - 2T_i^{*n}\right)}{\Delta x^{*2}} \tag{A19}$$

For Eq. (A6), an implicit differencing method is used, the form of the system of the implicit method follows as

$$\begin{bmatrix} B_{I_1+1} & C_{I_1+1} & & & & & \\ A_{I_1+2} & B_{I_1+2} & C_{I_1+2} & & & & \\ & A_{I_1+3} & B_{I_1+3} & C_{I_1+3} & & & \\ & & \cdots & & & & \\ & & & & A_{N-1} & B_{N-1} & C_{N-1} \\ & & & & & A_N & B_N \end{bmatrix} \times \begin{bmatrix} T_{I_1+1}^{*n+1} \\ T_{I_1+1}^{*n+2} \\ \cdots \\ \cdots \\ T_{N-1}^{*n+1} \\ T_N^{*n+1} \end{bmatrix} = \begin{bmatrix} D_{I_1+1} \\ D_{I_1+2} \\ \cdots \\ \cdots \\ D_{N-1} \\ D_N \end{bmatrix} \tag{A20}$$

where

$$A_i = -\frac{\Delta t^*}{\Delta x^{*2}}A_2 - \Phi_2\frac{k_2}{k_1}\frac{P_{2(i+1)}^* - P_{2i}^*}{\Delta x^*}\frac{\Delta t^*}{\Delta x^*} \tag{A21}$$

$$B_i = 1 + 2\frac{\Delta t^*}{\Delta x^{*2}} \tag{A22}$$

$$C_i = -\frac{\Delta t^*}{\Delta x^{*2}}A_2 + \Phi_2\frac{k_2}{k_1}\frac{P_{2(i+1)}^* - P_{2i}^*}{\Delta x^*}\frac{\Delta t^*}{\Delta x^*} \tag{A23}$$

$$D_i = T_{2i}^{*n} \tag{A24}$$

$$D_{I_1+1} = T_{2(I_1+1)}^{*n} + \left(\frac{\Delta t^*}{\Delta x^{*2}}A_2 + \Phi_2\frac{k_2}{k_1}\frac{P_{2(I_1+1)}^* - P_{2I_1}^*}{\Delta x^*}\frac{\Delta t^*}{\Delta x^*}\right)T_{2I_1}^{*n} \tag{A25}$$

$$D_N = T_{2N}^{*n} + \left(\frac{\Delta t^*}{\Delta x^{*2}} A_2 - \Phi_2 \frac{k_2}{k_1} \frac{P_{2N}^* - P_{2(N-1)}^*}{\Delta x^*} \frac{\Delta t^*}{\Delta x^*}\right) \times T_{2(N+1)}^{*n} \quad \text{(A26)}$$

Appendix B. Nomenclature and values of parameters

a,b,c	Empirical constants in Eq. (8)
a	0.0342 K^{-1}
b	0.0005 K^{-2}
c	6.4804
C_{P1}	Heat capacity of methane gas (2206 J/K·kg)
C_{P2}	Heat capacity of hydrate (1800 J/K·kg)
k_1	Phase permeability of gas in zone 1 (2.4 md)
k_2	Phase permeability of gas in zone 2 (0.6 md)
$\dot{m}_h$	Hydrate dissociation rate
T	Time
v_1	Velocity of natural gas in zone 1
v_2	Velocity of natural gas in zone 2
X	Distance
Z	Compressibility of gas (0.88)
A	Constant for calculate dissociation heat (− 1050 J/kg)
B	Constant for calculate dissociation heat (3,527,000 J/(kg K))
K_2	Heat conductivity of hydrate zone (3.4 J/(s m K))
P_0	Atmospheric pressure (1.01×10^5 Pa)
P_D	Hydrate decomposition pressure
P_e	Reservoir pressure at initial time (15 MPa)
P_G	Pressure at the well (MPa)
P_n	Pressure in zone 1 or 2
T_D	Hydrate dissociation temperature (K)
T_e	Reservoir temperature at initial time (K)
T_n	Temperature in zone 1 or 2
T_o	Reference temperature (273.15 K)
α	Water content of pores (0.15)
α_2	Heat diffusivity in hydrate zone (3.85×10^{-5} m^2/s)
β	Hydrate saturation of a layer (0.19)
ε	Mass fraction of gas in methane hydrate (0.129)
ρ_0	Density of methane gas at atmospheric pressure P_0 and temperature T_0 (0.714 kg/m^3)
ρ_1	Density of methane gas at gas zone
ρ_2	Density of methane gas at hydrate zone
ρ_3	Density of hydrate (0.91×10^3 kg/m^3)
ρ_W	Density of water (1.0×10^3 kg/m^3)
μ	Viscosity of gas (methane) (1×10^{-5} Pa S)
Φ	Porosity (0.2)
Φ_1	$(1-\alpha)\Phi$, content of free gas at zone 1
Φ_2	$(1-\beta)\Phi$, content of free gas at zone 2

References

Ahmadi, G., Ji, C., Smith, D.H., 2000. In: Holder, G.D., Bishnoi, P.R. (Eds.), A Simple Model for Natural Gas Production from Hydrate Decomposition, vol. 912. New York Academy of Sciences, New York, pp. 420–427.

Burshears, M., O'Brien, T.J., Malone, R.D., 1986. A multi-phase, multi-dimensional, variable composition simulation of gas production from a conventional gas reservoir in contact with hydrates. SPE 15246, Unconventional Gas Technology Symposium, Louisville, KY, May 18–21.

Collett, T., Lee, M.W., 2000. In: Holder, G.D., Bishnoi, P.R. (Eds.), Reservoir Characterization of Marine and Permafrost Associated Gas Hydrate Accumulations with Downhole Well Logs, vol. 912. New York Academy of Sciences, New York, pp. 51–64.

Durgut, I., Parlaktuna, M., 1996. A numerical method for the gas production process in gas hydrate reservoirs. 2nd International Conference on Natural Gas Hydrates, Toulouse, France, June 2–6, 1996.

Englezos, P., 1993. Reviews: clathrate hydrates. Ind. Eng. Chem. 32, 1251–1274.

Holder, G.D., Angert, P.F., Godbole, S.P., 1982. Simulation of gas production from a reservoir containing both gas hydrates and free natural gas. SPE 11005, 57th Annual Conference, New Orleans, Sept. 26–29.

Ji, C., Ahmadi, G., Smith, D.H., 2001. Natural gas production from hydrate decomposition by depressurization. Chem. Eng. Sci. 56, 5801–5814.

Kamath, V., 1983. Study of heat transfer characteristics during dissociation of gas hydrates in porous media. PhD thesis. University of Pittsburgh, Pittsburgh, PA.

Kim, H.C., Bishnoi, P.R., Heidemann, R.A., Rizvi, S.S.H., 1987. Kinetics of methane hydrates decomposition. Chem. Eng. Sci. 42, 1645–1653.

Makogon,Y.F., 1974. Hydrates of natural gas, Translated form Russian by Cieslesicz, W.J. Penn Well, Tulsa, OK.

Makogon, Y.F., 1997. Hydrates of hydrocarbons. Penn Well, Tulsa, OK.

Masuda, Y., Fujinaga, Y., Naganawa, S., Fujita, K., Sato, K., Hayashi, Y., 1999. Modeling and experimental studies on dissociation of methane gas hydrates in berea sandstone cores. 3rd International Conference on Natural Gas Hydrates, Salt Lake City, UT, July 18–22.

Moridis, G., Apps, J., Pruess, K., Myer, L., 1998. EOSHYDR: a TOUGH2 Module for ch_4-Hydrate Release and Flow in the Subsurface. Lawrence Berkeley National Laboratory, Berkeley, CA. LBNL-42386.

Selim, M.S., Sloan, E.D., 1989. Heat and mass transfer during the dissociation of hydrates in porous media. AIChE J. 35, 1049–1052.

Sloan, Jr., E.D., 1998. Clathrate Hydrates of Natural Gases, 2nd ed. Marcel Dekker, New York.

Swinkels, W.J.A.M., Drenth, R.J.J., 1999. Thermal reservoir simulation model of production from naturally occurring gas hydrate accumulations. SPE 56550, Annual Technical Conference, Houston, TX October, pp. 465–477.

Tsypkin, G., 2000. In: Holder, G.D., Bishnoi, P.R. (Eds.), Math-

ematical Models of Gas Hydrates Dissociation in Porous Media, vol. 912. New York Academy of Sciences, New York, pp. 428–436.
Verigin, N.N., Khabibullin, I.L., Khalikov, G.A., 1980. Izv. Akad. Nauk SSSR, Meh. Židk. Gaza 1, 174.
Yousif, M.H., et al., 1991. Experimental and theoretical investigation of methane-gas-hydrate dissociation in porous media. SPE Reserv. Eng., 69–76.